

# **A network model for natural ventilation simulation in deep buried underground structures**

**Yanan Liu<sup>a,d</sup>, Yimin Xiao<sup>a,b\*</sup>, Jianli Chen<sup>c</sup>, Godfried Augenbroe<sup>d</sup>, Tiecheng**

**Zhou<sup>a</sup>**

<sup>a</sup> Key Laboratory of the Three Gorges Reservoir Region's Eco-Environment, Ministry of

Education, Chongqing University, Chongqing 400045, China

<sup>b</sup> National Centre for International Research of Low-carbon and Green Buildings,

Chongqing University, Chongqing 400045, China

<sup>c</sup> National Renewable Energy Lab, USA

<sup>d</sup> School of Architecture, Georgia Institute of Technology, Atlanta, GA, USA

*\*Corresponding email: xiaoyimin@cqu.edu.cn*

Postal address: Faculty of Urban Construction and Environmental Engineering, Chongqing

University, Chongqing, 400045, China

## **Abstract:**

The study of underground natural ventilation opportunities has become increasingly significant in recent years with its promise of wide application in underground structures such as underground hydro power stations, metro stations, underground parking and laboratories. It is recognized that deployment of natural ventilation constitutes a passive technology that can lead to significant energy conservation if applied judiciously. This paper focuses on underground buildings that are buried deeply and typically consist of an underground complex network of connected structures. The other characteristic is that these structures house machinery and devices that generate

heat, leading to elevated internal air temperatures. Combined with the deep location, it implies that buoyancy forces are significant which make natural ventilation through vertical shaft openings a viable option. These characteristics demand a study of the heat transfer processes between ambient conditions, soil and underground buildings. In this paper, we present a dynamic flow network model with loops for multizone airflow and apply it to deep buried underground structures considering the dominant heat transfer characteristics, not only through the elements of the network but also the heat exchange with the envelope and adjacent soil mass. Finally, a small-scale experiment of occurring airflow is conducted and compared with the outcomes of the dynamic simulation of the proposed model. The comparison serves as validation and illustration of the application potential of the network model for natural ventilation investigation and consecutive optimization of its use in underground buildings.

**Keywords:** Network model; Heat transfer; Natural ventilation; Underground buildings

## Nomenclature

$A$	incidence matrix
$A'$	basic incidence matrix
$A_{jc}$	coefficient matrix of isothermal equations for node outflows
$A_{jr}$	coefficient matrix of heat balance equations for nodes
$A_e$	coefficient matrix of heat balance equations for elements
$A_{e1}$	coefficient matrix
$A_{e2}$	coefficient matrix
$A_1$	coefficient matrix
$A_2$	coefficient matrix
$1,ij$ and $2,ij$	sign functions
$C_f$	independent loop matrix

$c_p$	specific heat of air, 1.01 [kJ/(kg·K)]
$c_k$	coefficient of numerator in the transfer function
$d_k$	coefficient of denominator in the transfer function
$g$	gravitational acceleration, [m/s <sup>2</sup> ]
$l$	number of terms of the numerator
$m$	number of terms of the denominator
$M$	n-dimensional column vector
$M_j$	Mass flow rate of the $j^{th}$ element
$\Delta P_{r,j}$	flow resistance of element j, [Pa]
$\Delta P_r$	flow resistance matrix
$P_d$	pressure rise matrix
$P_w$	wind-induced pressure, [Pa]
$P_f$	mechanical fan pressure, [Pa]
$P_{e,j}$	Air pressure at the element outlet, [Pa]
$P_{s,j}$	Air pressure at the element inlet, [Pa]
$P_{tj}$	thermal buoyancy pressure of element j, [Pa]
$Q_{w,j}$	heat gain through the envelope of the $j^{th}$ element
$Q_{,j}$	heat released from equipment in the $j^{th}$ element
$Q_{A,j}$	heat removed by air conditioning in the $j^{th}$ element
$Q_0$	1 × n vector
$q_{di}$	heat flux, [W/m <sup>2</sup> ]
$q_{nij}$	heat flux, [W/m <sup>2</sup> ]
$q_y$	heat flux, [W/m <sup>2</sup> ]
$t_{ij}$	the air temperature at hour j of day i, [°C]
$\bar{t}_y$	yearly mean air temperature, [°C]
$\bar{t}_{di}$	mean air temperature of day i, [°C]
$t_0$	ambient air temperature, [°C]

$s$	column vector for the temperature of start points of all elements from 1~n
$t_{sj}$	air temperature of the starting point in element $j$
$e$	column vector for the temperature of end points of all elements from 1~n
$t_{ej}$	air temperature of the end in element $j$
$t_{t,j}$	air temperature of element $j$ in an infinitesimal section, [°C]
$r_{jn}$	mean air temperature of the element $j$ at time step n
$r_{j(n-1)}$	mean air temperature of the element $j$ at time step n-1
$U_j$	volumetric flow impedance coefficient of the $j^{th}$ element, [m <sup>-4</sup> ]
$V_j$	volume of element $j$ , [m <sup>3</sup> ]
$\Delta Z$	vertical difference between inlet and outlet of the element, [m]
$dz$	height difference in differential form, [m]
$\rho_0$	ambient air density, [kg/m <sup>3</sup> ]
$\rho_j$	air density of $j^{th}$ element, [kg/m <sup>3</sup> ]
$\Delta\tau$	time step interval
$\omega_y$	angular frequency for the yearly temperature variety wave
$\omega_d$	angular frequency for the daily temperature variety wave

## 1. Introduction

Airflow simulation has become mature over the last decades and is now a significant aid for designers and engineers to better evaluate the ventilation performance of buildings, both aboveground and underground. In current practice, the methods and tools to study airflow patterns under different scenarios have become mainstream. This has added significantly to more rigorous performance assessments of above-ground building designs, indoor air quality, as well as ventilation efficiency of underground spaces and so on [1-6].

With the advancement of our society and city infrastructures in particular, humans have built an increasing amount of underground facilities, such as metros, hydro power stations, laboratories and other entertainment space etc. How to make an efficient usage of these underground spaces with respect to the expected environment related to worker comfort, but also the energy efficiency, has become a concern for city planners. Especially for large underground facilities such as hydro power stations, the energy demand for mechanical cooling is excessive considering the significant heat emission from heat sources such as power generators during operation. In this sense, making efficient use of natural ventilation for underground spaces ventilation and environment adjustment and obtain "free" cooling has attracted increasing attention. For these and many other purposes, designers and engineers are conducting airflow simulations at different resolutions dependent on the project requirements as well as time and budget constraints. Hence, to satisfy the varying needs and meet the restrictions of available computing power, numerous competing models have been developed. They are multiple classifications that help to understand the differences between various models [7], e.g. analytical, empirical, experimental, multizone, zonal, and Computational Fluid Dynamics (CFD), are the labels that apply. The different model types vary in their computational complexity and prediction accuracy. This will be elaborated below.

Starting with the simplest approaches, either analytical or empirical models are derived from analysis and simplification of the theoretical equations of the physics of fluid dynamics and heat transfer. Providing fast and approximate evaluation of ventilation performance, analytical and empirical models are primarily useful for a quick assessment in the early stages of ventilation design practice. The inherent simplifications and approximations in the model development limit their application typically to a similar class of cases with a limited scope to ensure acceptable prediction accuracy [8]. An example of this is a model that predicts the natural ventilation rate in a single-zone with two openings [9]. Another example is a model that captures the relationships between flows, pressure differential and effective leakage area (ELA) of

an enclosure [10]. In addition to analytical models, researchers have also developed empirical airflow models from experimental data. Based on the scale of the experiment, these experimental models could further be divided into small-scale and full-scale experimental models [8]. The two different scales of experiments, e.g. a small size physical set-up in the laboratory or a full-scale experiment on actual sites, can deliver approximate but in most cases reliable results for ventilation performance evaluation. But the scaling of certain thermal fluid characteristics makes the small-scale experimental models hard to generalize to full scale reality. On the other hand, the full-scale experiments are typically too expensive to run. This explains the frequent use of small-scale set-ups for the validation of simulation models that can consequently be used at the full scale under certain restrictions.

Particularly popular models for ventilation design are so-called multizone models. They are used for a multitude of applications in the building industry. Multizone models predict the airflow patterns in buildings by solving the mass and energy equations. The momentum of air is neglected in this type of model. In addition, the model assumes the air is well mixed in each zone such that a zone can be efficiently represented by uniformly defined physical parameters, e.g. a single air temperature, pressure and relative humidity for the whole zone. Feustel et al. [11] conducted a survey in which they looked at 50 multizone models as among which the well-known COMIS, CONTAM, AIRNET, BREEZE. They are widely applied in aboveground building simulations. COMIS is one of the first multizone models used for airflow prediction that comprises a module for calculation of the normalized wind pressure coefficients at the facades of the building [12-14], which is essential for the calculation of the momentary airflows through a façade for a given wind velocity and direction. It should be noted that some of the above models support only a limited integration of the thermal and flow model. In those cases, the nodal temperatures are supplied as prior known inputs to the flow simulation. This is obviously an unsatisfactory approach if the temperature behavior is strongly coupled with the flows in which case the co-simulation

of flows and temperatures are a requirement.

Haghighat F. & Megri A.C. [15] conducted a comprehensive validation of COMIS and CONTAM, the results showing good agreement between them. COMIS was integrated with an indoor aerosol dynamic model (MIAQ4) to predict particle dispersion in a three-room chamber. SF6 and environmental tobacco smoke particle concentrations were released in the chamber and measurements compared with model predictions [16]. To obtain the detailed air flow and particle distribution in a specific zone, several researchers have integrated CFD with existing multizone models [17-22]. As another example, Gang Tan [23] developed a multizone coupled heat transfer and natural ventilation nodal model called multiVent. It calculates indoor air temperatures in response to weather data and internal heat loads and has a web-based input facility. MultiVent was integrated with CFD to study the natural ventilation driven by wind and buoyancy. Other authors developed a state-space method as a complementary method for solving concentration dynamics within multizone software [24]. Based on the classification by Axley [25], there is an alternative to the nodal models such as COMIS and CONTAM mentioned above. Axley introduces a category of multizone network models, which he calls the loop model. It has been used for the analysis of hydraulic networks [26] and mine shaft ventilation [27, 28]. For example, Fytas et al. [27, 28] introduced an integrated mine ventilation design software that could be applied in ventilation network analysis with focus on the design of active fan systems. The loop method is based on graph theory, which can easily identify complicated loops and conduct network topology analysis. Jensen et al [29] integrated a thermal program with an existing multizone airflow network model based on the loop method. Validations were carried out to demonstrate its ability to predict complex airflow patterns. It seems that the loop method has been overlooked by most of members in the building simulation community [25].

A recap of the published works reveals that amongst all flow simulation approaches, CFD is quite popular in aboveground buildings, but it is less suitable for underground

networks where the complex configuration will become a bottleneck in the preparation. This is due to the difficulty to build the geometric model and define appropriate boundary conditions, which typically leads to increased modeling effort and computation time. Therefore, it is worthwhile to develop a suitable simulation model that could deal with the complex underground structures without these demands on valuable resources. The obvious choice is to adapt existing network models to be applicable to the specific underground configurations and use the Bernoulli equation to describe the airflow. If successful, it provides a simple and straightforward method that is easy to use compared with a CFD approach. Obviously, it will have to be proven that the network model provides an approximation of ventilation rates for each zone that are adequate to guarantee proper designs.

The ventilation of underground spaces has been researched for application in various fields, including the underground hydro power station, mine ventilation, metro system and others. For example, Li et al. [30] conducted a field test to study the thermal pressure in a traffic tunnel of a hydro power station and derived an empirical equation to predict thermal pressure under different circumstances. Also, Li et al. [31] investigated the influence of supply air velocity and heat release rates on the air distribution within the powerhouse of a hydro power station. The experimental results are useful for optimizing the air distribution design in large underground spaces, for instance to model the heat and moisture transfer in the tailrace tunnel of hydro power stations, Yu et al. [32] developed a quasi-three-dimensional mathematical model based on the airflow analysis and validated the model using the field test data from one hydro power station. Liu et al. [33] proposed a numerical model based on reformulated RNG  $k-\varepsilon$  model to simulate the ventilation of powerhouses of the Xiluodu hydro power station. The accuracy of the simulation was verified using field data. Although significant works exist to study ventilation of hydro power stations, all studies are limited to the investigation of heat and mass transfer for single zone of a hydro power station, such

as the powerhouse, traffic tunnel and tailrace tunnel as mentioned above. Similar to the case of mine ventilation, fan systems including a single fan or multiple fans are typically used to maintain sufficient air exchange rate [34]. To model the mine ventilation status, besides the methods [27, 28] mentioned above, Szlázak et al. [35] proposed to model the air distribution of mine ventilation using a graph-based ventilation network consisting of nodes and arcs. The arcs in the network represent one-dimensional flow modeled with basic fluid dynamics equations. Although equipped with the capability of simulating multizone airflow for mine ventilation applications, these models neglect the thermal-driven ventilation since the air pressure caused by fan operation is typically the main force that drives the airflow in the absence of significant heat emission sources. In addition, to study the airflow in metro spaces, researchers developed software such as SES (subway environmental simulation) to model airflow and pressure fields [36]. However, this software is specifically designed for simulating the airflow in metro tunnels considering the uniqueness of the piston effect [37, 38] from moving trains in these spaces.

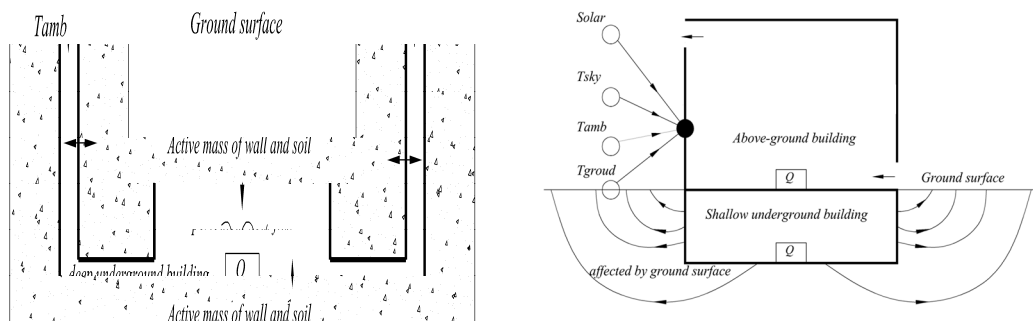


**Fig.1.** Schematical comparison between underground building and aboveground building.

As a summary, in spite of the available results from the works mentioned above, there still exists gaps in predicting airflow in underground structures. Unlike aboveground buildings that have an envelope system with finite thickness to separate indoor and outdoor environment, and hence has some degree of leakiness, the envelope system of underground spaces can be considered as infinitely thick and without air leakage since it is in direct contact with the soil and rocks around [39]. This of course

influences the heat exchange processes of deep buried spaces with their surrounding mass. More specifically, the large active mass in the structure and adjacent soil renders the dynamics of the heat exchange with the surroundings very gradual, as the conceptualization in Fig.1 illustrates. The special demands of airflow models for underground structures are related to their special geometries (many zones of varying size and connected in complex layouts) and many localized heat emission sources. These characteristics make nodal methods with the assumption of well-mixed air within each zone not suitable, as this assumption does not reflect the special geometries such as long tunnels where the flow predominantly happens along the length of the tunnel, thus resembling duct flow with directional temperature variation, rather than a zone with mixed air and uniform temperature. As remarked earlier, the other alternative, CFD, is too computationally intensive for these large structures with the additional complexity that the many boundary conditions are hard to model correctly. Overall speaking, there exist no proven model that is suitable to simulate complex multizone airflow with thermal buoyancy effects for large underground structures. Based on our literature review, all existing models carry their own characteristics that make them specific purposes (such as airflow investigation for selected functional zones in hydro power stations, mine ventilation and metro airflow simulation). Hence, in this paper, we propose to use the loop method with continuous temperature distribution for each loop element and couple it with the Z-transfer method [40] to simulate multizone airflows. Currently, the loop method has mostly been applied to simulate airflow in aboveground spaces. As referred to earlier, full integration of the flow model with the thermal model is a priority for our approach, especially considering the heat transfer characteristics of airflows through long tunnel shape spaces. For the latter, the proposed method assumes a piecewise linear temperature variation along the airflow path. If proven accurate enough, the proposed approach can be utilized to simulate multizone airflow in any underground configuration complexity.

## 2.The description of underground natural ventilation model

The proposed model is a loop-based network model consisting of nodes and elements. The loop concept is used to convert physical models into mathematical expressions. By using the loop concept, the geometrical and topological relations of the loop networks are represented by the incidence matrix and independent loop matrix. The theory part below presents how the loop method is used to set up the governing equations and solve the airflow and thermal coupling problem.

### 2.1 The concept of the loop-based network model

#### 2.1.1 Definition of element and node

The tunnels and rooms in the underground facility are divided into elements that connect with each other. Heat transfer and airflow pressure/mass balances are considered in the elements simultaneously. Fig.2 is the schematic diagram of an element. Some basic assumptions are made for the element: (1) same volume as the actual space; (2) one-dimensional airflow (constant mass flow along the path, pressure balance between pressure changes and flow resistance, heat balance); (3) Linear distribution of air temperature along the length.

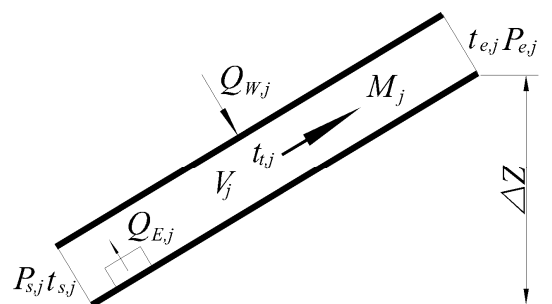


Fig. 2. Schematic of an element.

A Node is the endpoint of an element. Some assumptions are made concerning a node: (1) no volume; (2) no temperature; (3) one pressure value; (4) well-mixing condition

when multiple airflows come together in a node.

### **2.1.2 The division of a long tunnel into elements**

Due to heat transfer between the moving air and surfaces of the enclosures, the temperatures and densities will vary in a tunnel, and when the tunnel is long the variation will be significant. Along the direction of airflow, the heat transfer will gradually decrease as temperature difference between the air and wall surfaces will get smaller. This fact leads to the non-linear change of air temperature along the tunnel. It has been proven that the temperature distribution is an exponential function along the length [41-43]. To simplify, we divide a long tunnel into several elements that connect with each other. We assume linear temperature variation for each small element, so that we can calculate the heat transfer, air temperature and thermal buoyancy pressure within acceptable accuracy.

### **2.1.3 The elements division of underground rooms**

Deep-buried underground spaces are usually capacious in order to accommodate different types of large and heavy equipment. The spaces are connected with other long tunnels and rooms thus having multiple air inlets and outlets. Since one element only contains two nodes, only a space with two openings can be simplified as one element. In order to reflect the air temperature distribution inside the space as accurately as possible, sometimes it is necessary to divide the space into several elements. The principle of elements division is to match the actual heat transfer, ventilation flow and temperature distribution within a space as much as possible.

### **2.1.4 The virtual element for outdoor air**

Several tunnels will have openings connected with outdoor air. With varying locations

and altitude, it is not reasonable to use only one node to represent the status of the outdoor air. By connecting all separate nodes with virtual elements, we assume that the air can flow from one tunnel into another through these virtual elements to ensure the conservation of mass, heat balance and pressure balance in the network model. In these virtual elements, the thermal buoyancy pressure and flow resistance are all taken to be zero.

With virtual elements, the heat gain from underground spaces is released to the outdoor environment to ensure the heat balance of the model, i.e. the temperature of outdoor virtual elements is always equal to the outdoor air temperature at the corresponding locations. When the height of different entrances into a long tunnel are significantly different, the corresponding temperature should be adjusted with the altitude. The temperature will decrease when the altitude increase. Environmental lapse rate [typically assumed to be  $-0.65\text{ }^{\circ}\text{C (100m)}^{-1}$ ] is used to modify the air temperature [44].

### **2.1.5 The formation of the network model based on elements**

Based on the method stated in section 2.1.2-2.1.4, deep-buried tunnels, underground rooms and the connected outdoor environment is converted into elements first. Then the ventilation network is formed by connecting the elements based on their physical relations. As indicated in the example of Fig.3a, this deep-buried large space is connected with three long tunnels, each of which is further divided into several connected elements. The large space is divided into three elements as indicated in Fig.3b. Independent loops are constructed as illustrated in Fig.3c. When there are  $u$  number of nodes connected with outdoor air,  $u-1$  virtual elements are required [45]. As long as all virtual elements form a tree, the manner in which they are connected can be flexible.

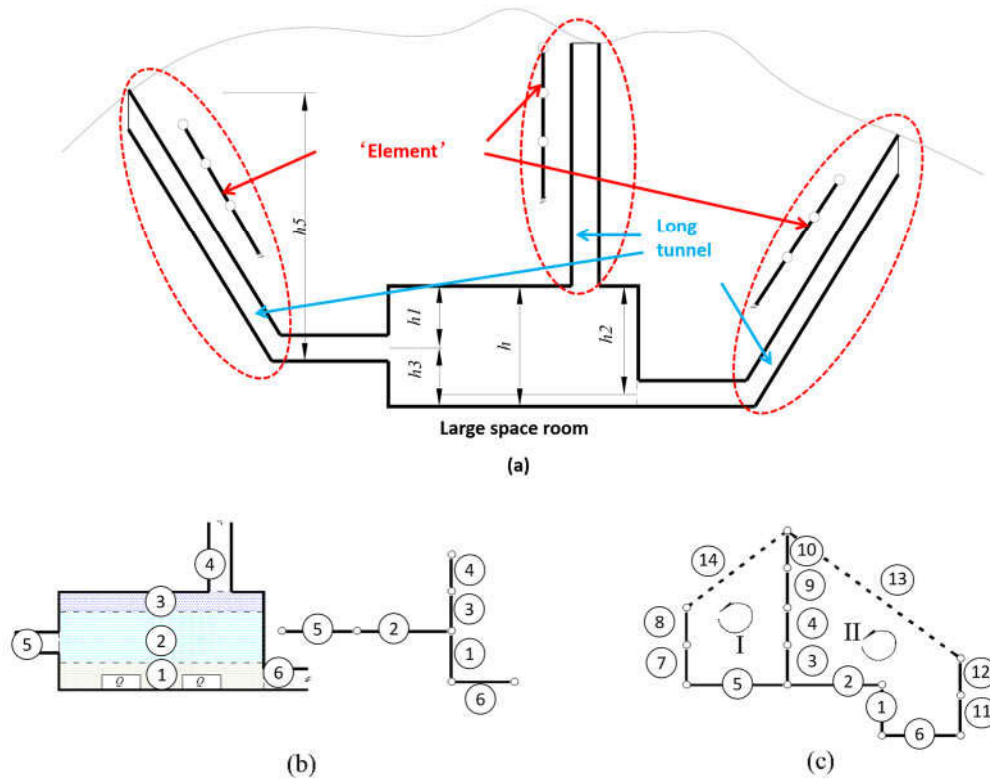


Fig. 3. A typical natural ventilation network of deep-buried underground building.

## 2.2 Mathematical equations for the loop-based network model

In the network model, the basic parameter is the mass flow rates  $M$  for each element. If there are  $n$  elements in the ventilation network (including outdoor virtual elements), the mass flow rates  $M$  contains  $n$  unknowns. Firstly, we describe the establishment of the governing equations for solving the mass flow rates of the elements, which consists of the mass flow rates balance equations of nodes (Eq.2-1) and the pressure balance equations of loops (Eq.2-2). The thermal pressure of elements in the loop pressure balance equations are determined by the air temperature distributions of the elements. This paper presents the calculation model of the air temperature  $T$  of elements, including equations (Eq.2-7, Eq.2-12 and Eq.2-13). In the air temperature calculation equations of elements, there are two parameters, mass flow rates  $M$  of the elements and heat transfer  $Q_w$  between the elements and the envelope. Hence, the  $z$  transfer method is introduced to calculate the heat transfer  $Q_w$ .

The description above shows that the air mass flow rates  $M$ , air temperature  $T$  and heat transfer  $Q_w$  of the envelope structure are coupled.

### 2.2.1 Mass flow balance equations of nodes

In the network model, nodes and elements constitute multiple closed-loops, and every node is connected with multiple elements. The sum of mass flow rates in all elements that connected to the same node is equal to zero. Assuming that there are  $m$  nodes in the network, any  $m-1$  equations in the mass flow balance equations is linearly independent, and constitutes the mass flow balance equations of nodes.

The mass flow balance equations of nodes in a network are expressed as:

$$A' \times M = 0 \quad (2-1)$$

Where  $A'$  is the basic incidence matrix with the dimension of  $(m - 1) \times n$ ,  $M$  is an  $n$ -dimensional column vector with each element  $M_j$  ( $j= 1 \sim n$ ) representing the mass flow of element  $j$ .

### 2.2.2 Pressure balance equations of loops

For each element, the pressure balance equations of its two endpoints (nodes) can be established. Considering that the ventilation network is composed of closed-loops, the pressure equation of each element is superimposed along the closed loop to obtain the pressure balance equation of the loop. In any independent loop, the sum of the total pressure rise and the total flow resistance is equal to zero, given by:

$$C_f \cdot (\Delta P_r - P_d) = 0 \quad (2-2)$$

Where  $C_f$  is  $(n - m + 1) \times n$  independent loop matrix,  $\Delta P_r (n \times 1)$  is the flow resistance matrix, and  $P_d (n \times 1)$  is the pressure rise matrix.  $P_d = P_t + P_w + P_f$ .

$P_t$  is thermal buoyancy pressure calculated using Eq.2-4,  $P_w$  is outdoor wind pressure that has impacts on the pressure of element connected to outdoor [46],  $P_f$  is mechanical fan power that is determined by the fan performance curve.

Above (2-1) contains  $m-1$  equations, (2-2) contains  $n-m+1$  equations, and the total number of equations is  $n$ , which constitutes the governing equations for solving the unknown mass flow rates of  $n$  elements, but the supplementary equations for  $\Delta P_r$ ,  $P_t$ ,  $P_w$  and  $P_f$  are still needed.

The flow resistance in each element is written as:

$$\Delta P_{rj} = \frac{U_j}{\rho_j} M_j^2 \quad (2-3)$$

Where  $U_j$  is the volumetric flow impedance coefficient, which is determined by the friction losses and local losses,  $m^{-4}$ .

The buoyancy pressure of an element is defined as the pressure difference driven by the density difference between internal space and external space of the element. The buoyancy pressure is determined by the temperature distribution of an element.

$$P_{tj} = \int_j (\rho_0 - \rho_j) g \cdot dz = \int_j \rho_0 \left( 1 - \frac{27315+t_0}{27315+t_{tj}} \right) g \cdot dz = \rho_0 \left( 1 - \frac{27315+t_0}{27315 + \frac{t_{sj} + t_{ej}}{2}} \right) g \cdot \Delta z \quad (2-4)$$

It can be seen that under the assumption of linear temperature distribution, the element's thermal pressure can be calculated by the air temperature at the inlet and outlet of the element.

### 2.2.3 Air Temperature Calculation Model of Elements

As mentioned above, in order to calculate the thermal pressure of elements, it is necessary to establish supplementary equations for calculating air temperature.

Considering that the mass conservation equations are expressed in matrix form, in order to make the established equations consistent, we will derive the matrix form of the air temperature calculation equations in detail.

### 2.2.3.1 The vector of element temperatures $T$

These temperatures of the inlet and outlet of an element are arranged in sequence to form the temperature column vector  $T$ .

$$T = \begin{bmatrix} T_s \\ T_e \end{bmatrix} \quad (2-5)$$

Where  $T_s$  is the column vector for the temperature of the start points of elements from 1~ $n$   $T = [t_{s1}, t_{s2}, \dots, t_{sn}]'$ .  $T_e$  is the column vector for the temperature of the end points of elements from 1~ $n$   $T_e = [t_{e1}, t_{e2}, \dots, t_{en}]'$ . Thus,  $T$  has  $2n$  entries. Also, there are  $u-1$  outdoor virtual elements whose inlet temperatures are prescribed as the outdoor temperature. They have to be deducted, so there are  $2n-u+1$  unknowns in total.

### 2.2.3.2 Heat balance equations for airflows mixing process at the node

Since there is no volume for the node, the total enthalpy that enters into the node is equal to enthalpy leaving from it. Which is written as:

$$\sum_{j=1}^n x_{1ij} c_p |M_j| t_{sj} + \sum_{j=1}^n z_{ij} c_p |M_j| t_{ej} = 0, \quad i = 1 \sim m \quad (2-6)$$

Where  $c_p$  represents the specific heat of air, in  $1.01 \text{kJ}/(\text{kg}\cdot\text{K})$ ;  $x_{1ij}$  and  $z_{ij}$  are sign functions. If the flow in the  $j^{\text{th}}$  element is from the node  $i$ ,  $x_{1ij} = 1$ , otherwise,  $x_{1ij} = 0$ . If the flow of the  $j^{\text{th}}$  element enters into the node  $i$ ,  $z_{ij} = -1$ , otherwise,  $z_{ij} = 0$ .

Eq.2-6 can be written in matrix form as follows:

$$A_{jr} \cdot T = 0 \quad (2-7)$$

Where

$$A_{jr} = [A_{je}; A_{ji}] \quad (2-8)$$

Where  $A_{jr}$  is a  $m \times 2n$  matrix with a rank of  $m$ , and its derivation is shown in Appendix A. Eq.2-7 has  $m$  mutually independent equations.

### 2.2.3.3 Heat balance equations of elements

Considering heat transfer by airflows, internal heat sources and the internal surface of walls, the heat balance equation for an element is written as:

$$Q_{wj} + Q_j + |M_j| \cdot c_p (t_{sj} - t_{ej}) - Q_{Aj} = V_j \cdot \rho_j \cdot c_p \cdot \frac{T_{rjn} - T_{rj(n-1)}}{\Delta\tau} \quad (2-9)$$

Where  $Q_{wj}$  is heat gain, which is modeled by the Z-transfer coefficient method [37], from the envelope of underground structure on the  $j^{th}$  element ;  $\Delta\tau$  represents the time step interval.

The arithmetic mean of the start and end of an element is used as the average temperature of that element. Omitting the subscript  $k$ , Eq.2-9 could be written as:

$$\left( |M_j| \cdot c_p - \frac{V_j \rho_j c_p}{2\Delta\tau} \right) t_{ej} - \left( |M_j| \cdot c_p + \frac{V_j \rho_j c_p}{2\Delta\tau} \right) t_{sj} = -Q_{wj} - Q_j - \frac{V_j \rho_j c_p T_{rj(k-1)}}{\Delta\tau} \quad (2-10)$$

Assuming  $A_{e0} = [A_{e1} \ A_{e2}]$

Where  $A_{e1} = \text{diag}\left[ \left( |M_j| \cdot c_p - \frac{V_j \rho_j c_p}{2\Delta\tau} \right) \right]$ ,  $A_{e2} = -\text{diag}\left[ \left( |M_j| \cdot c_p + \frac{V_j \rho_j c_p}{2\Delta\tau} \right) \right]$ ,

$$Q_0 = [q_1, q_2, \dots, q_n]', \quad q_j = -Q_{wj} - Q_{Ej} - \frac{V_j \rho_f c_p (T_{j(k-1)} - T)}{\Delta \tau}, \quad j = 1 \sim n.$$

Written in the matrix form, Eq.2-10 becomes:

$$A_{e0} \cdot T = Q_0 \quad (2-11)$$

Obviously, if  $\text{rank}(A_{e2}) = n$ , then we can get  $\text{rank}(A_{e0}) = n$ . Thus, Eq.2-11 includes  $n$  equations, which are mutually independent. Since the outdoor temperature is prescribed, the balance equations for outdoor virtual elements should be deleted. After deleting corresponding rows,  $A_{e0}$  can be converted to  $A_e$  while  $Q_0$  can be converted to  $Q$ . Eq.2-11 can be changed to:

$$A_e \cdot T = Q \quad (2-12)$$

Where there exists  $n-u+1$  mutually independent equations.

#### 2.2.3.4 Supplementary isothermal equations for multiple elements starting from the same nodes

Assuming that the airflow at nodes can quickly reach a fully mixed state, when the starting points of several elements are the same, the air temperature entering these elements is equal. If the airflow leaves from one node to 3 elements (e.g.  $e_2, e_3, e_4$ ), two isothermal equations could be obtained:

$$\begin{cases} t_{s2} - t_{s3} = 0 \\ t_{s2} - t_{s4} = 0 \end{cases} \text{ or } \begin{cases} t_{s2} - t_{s3} = 0 \\ t_{s3} - t_{s4} = 0 \end{cases}$$

For the  $i^{\text{th}}$  node, if it has  $k_i$  outflow elements, the number of isothermal equations of that node outflow is calculated as:

$$\sum_{i=1}^m (k_i - 1) = \sum_{i=1}^m k_i - m = n - m$$

The isothermal equations for these nodes can be expressed in a simplified matrix form, given by:

$$A_{jc} \cdot T = 0 \quad (2-13)$$

Where

$$A_{jc} = [A_{jc1}; \text{zeros}(n - mn)] \quad (2-14)$$

And  $A_{jc}$  is a matrix of order  $(n - m) \times 2n$ . The mathematical derivation of  $A_{jc}$  is shown in Appendix B.

Eq.2-7, Eq.2-12 and Eq.2-13 form the temperature network model. There are  $2n-u+1$  linear equations and unknown temperatures. When we know the airflow rates and heat transfer of each element, these equations can be solved.

#### 2.2.4 Envelope heat transfer model

In the natural ventilation of an underground space, since the internal air temperature is uncontrolled, the heat transfer between surface of the envelope and internal air is complicated. When underground spaces are buried deeper than 12 m, the impact of ambient temperature fluctuation can be neglected. This type of building is called the deep-buried underground building. In this scenario, the variation of soil temperature is only caused by the fluctuation of internal air temperatures in the underground spaces  $t_n(\tau)$ . This fluctuation of air temperature makes the heavy and dense envelope accumulate and release heat over time. Through the dynamic heat transfer process, the air temperature  $t_n(\tau)$  is affected accordingly. This dynamic heat exchange and coupling between air and envelop should obviously be covered by the computational model.

Although  $t_n(\tau)$  is a continuous function of time, in practical engineering problems, we simplify it by utilizing the time series function  $\{t_{ij}\}$  with time interval of 1 h as approximation.  $\{t_{ij}\}$  is mainly affected by the outdoor air temperature and thermal disturbance from the adjacent space. Based on the fluctuation of daily mean temperature and yearly mean temperature,  $\{t_{ij}\}$  can be written as:

$$t_{ij} = \bar{t}_y + (\bar{t}_{di} - \bar{t}_y) + (t_{ij} - \bar{t}_{di}), \quad i = 1 \sim 365 \quad j = 1 \sim 24 \quad (2-15)$$

In the formula above,  $\bar{t}_y$  is a constant for the whole year,  $\bar{t}_{di} - \bar{t}_y$  changes daily, representing the dominant harmonic of yearly temperature fluctuation. The corresponding angular frequency  $\omega_y = 19924 \times 10^{-7} s^{-1}$ .  $t_{ij} - \bar{t}_{di}$  changes hourly, which is the dominant harmonic of the daily temperature fluctuation. The corresponding angular frequency  $\omega_d = 72722 \times 10^{-5} s^{-1}$ . According to the superposition principle of linear systems, the hourly heat flux  $q_{ij}$  of envelope with the impact of  $t_{ij}$  is written as:

$$q_{ij} = q_y + q_{di} + q_{hij} \quad (2-16)$$

Where  $q_y$  is the heat flux between the air with yearly mean temperature and the envelope with constant temperature,  $W/m^2$ .  $q_{di}$  is the heat flux corresponding to  $\bar{t}_{di} - \bar{t}_y$ , which changes day by day,  $W/m^2$ .  $q_{hij}$  is the heat flux corresponding to  $t_{ij} - \bar{t}_{di}$ , which changes hourly,  $W/m^2$ .  $q_y$  can be obtained by an analytical method [39]; in the calculation,  $q_y$  attenuates fast. It becomes negligible after one year. The calculation of transient heat transfer through the envelope driven by the temperature harmonic  $\bar{t}_{di} - \bar{t}_y$  and  $t_{ij} - \bar{t}_{di}$  uses the time series based Z-transfer coefficient method [40]. The fluctuation of temperature wave  $\bar{t}_{di} - \bar{t}_y$  and  $t_{ij} - \bar{t}_{di}$  will make the envelope absorb and release heat alternatively. Different frequencies of the temperature harmonics will affect the “active” thickness of the envelope that is involved in this heat absorption and release process. With a lower frequency of the temperature wave (thus longer period),

its impact on heat transfer reaches a deeper position of the envelope. With a higher frequency (thus shorter period), its impact on heat transfer reaches a shallower position of the envelope. Hence, the transfer function of the two temperature harmonics is different, and should be calculated separately.

Assuming  $\tilde{t}_{di} = \bar{t}_{di} - t_y$ , the heat flux  $q_{di}$  from room air to internal surface driven by  $\tilde{t}_{di}$  is written as:

$$q_{di} = \sum_{k=0}^l c_k \tilde{t}_{d(i-k)} - \sum_{k=1}^m d_k q_{d(i-k)}, \text{ if } i < k_j = i + 365j = 1 \sim 365 \quad (2-17)$$

The time interval is set as 1 day when calculating  $q_{di}$ .

Assuming  $\tilde{t}_{ij} = t_{ij} - \bar{t}_{di}$ , the heat flux  $q_{hij}$  from room air to internal enclosure surface driven by  $\tilde{t}_{ij}$  is written as:

$$q_{hij} = \sum_{k=0}^l c_k \tilde{t}_{i(j-k)} - \sum_{k=1}^m d_k q_{hi(j-k)} \text{ if } j < k_j = i + 24j = i - 1j = 1 \sim 24 \quad (2-18)$$

The time interval is set as 1 hour when calculating  $q_{hij}$ .

### **2.3 Coupled computation of envelope heat transfer $Q_w$ , air temperature $T$ and airflow rates $M$**

To predict the natural ventilation status of underground buildings using the proposed network approach, the required input parameters include the geometrical dimensions and topological relations of elements, thermal property of envelopes, the space layout, capacity, the operation schedule of heat sources and annual hourly weather data. The unknown parameters include air temperatures of the elements, heat transfer between envelopes and internal airflow, and airflow rates. Their coupling relations are shown in Fig.4.

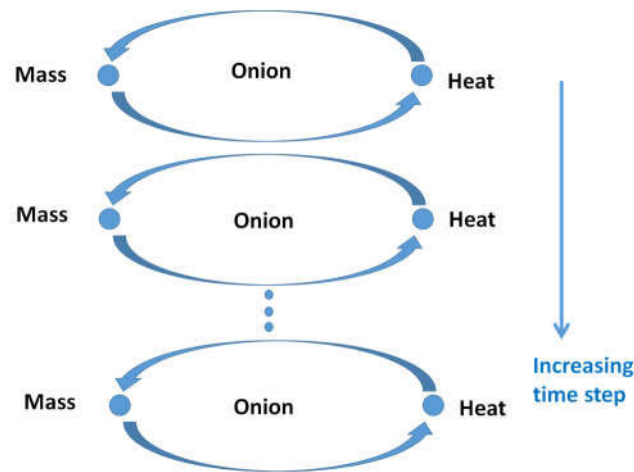


**Fig. 4.** Coupling between unknown parameters.

The onion method is adopted to reflect the interaction between airflows and heat transfer as recommended by [29]. In the coupling, through algebraic operations and repeated iterations between the calculation of thermal network model and flow network flow model, the computation will proceed to next time step when convergence is reached.

In the network flow model, the pressure balance equations of independent loops are nonlinear, which is solved by the Newton downhill method [47, 48].

The envelope of deep buried structures is composed of heavy rocks and soil. The time span of heat transfer through these materials could be up to one year or even longer. As mentioned in the previous section, each time step in the calculation involves time-consuming algebraic operations and repeated iterations, hence, a “Double layer time step” simulation strategy is adopted to minimize the computational time. First, we calculate the daily mean ventilation status and thermal environment status for each day of a year. Then, based on these daily results, we conduct the hourly calculation for predicting the natural ventilation status. The procedures for calculating hourly results and daily results are similar.

The diagram of the complete multizone airflow calculation process is illustrated in the Fig.5 below. Firstly, we should prepare input parameters of the model including the labels of the nodes and elements, flow impedance coefficient, heat sources strength and locations, thermal properties of elements, operation schedule of heat sources etc. In

addition, we also need to form the matrix of the network model and compute the Z-transfer coefficient of the envelope as the prepared inputs for the network flow calculation. Then, as the third step, we implement the onion method mentioned above to integrate airflow rates and thermal heat transfer calculation. Temperature unknowns of the elements are the basic parameters for the thermal network model, while the mass flow rates are the basic parameters for the flow network model. The algorithm shows how these parameters are obtained by solving the corresponding governing equations as indicated in the third portion of Fig.5. Finally, we proceed to the next time step and repeat the whole process of calculation.

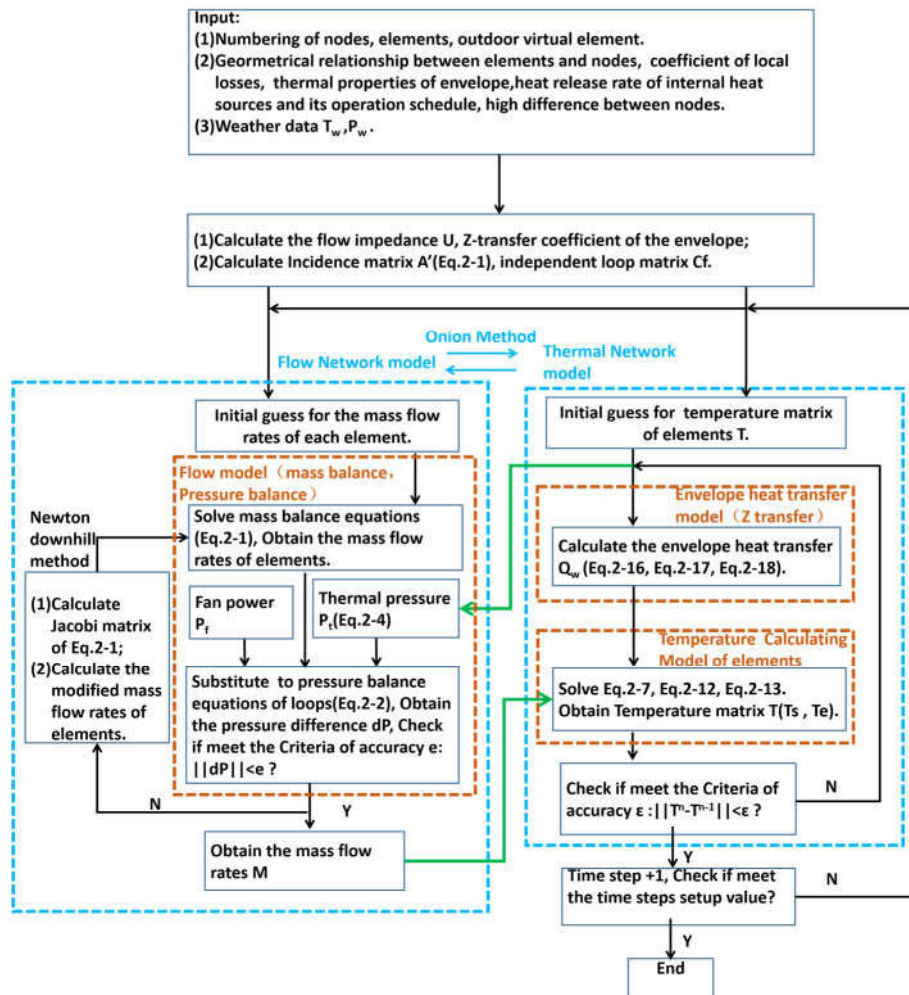


Fig. 5. Diagram of the solution process.

### **3.Experimental validation**

To validate our proposed model, we have conducted the validation using two experiments, i.e., one small-scale model experiment and one field measurement in a tunnel. With heat sources inside elements, the small-scale experiment was mainly designed to validate the flow model and the integration between internal heat sources and airflow. Furthermore, because it is not practical to simulate the real deep-buried environment in the laboratory, the field measurement was employed to validate the heat transfer model between the airflow and deep rocks.

#### **3.1 Flow model validation**

The small-scale experiment was conducted first to validate the flow model and its integration with internal heat sources when underground spaces are in natural ventilation mode. A 1:20 scale model of a real underground hydro power station was constructed for the experiment. As shown in Fig.6, it is a typical design of power station with a deep buried power generator room, transformer hall, busbar corridors, equipment hoisting shaft, high voltage cable shaft and transportation channel etc. In the station, there exist six power generators and six busbar corridors in total. Meanwhile, the hydro power station also has 4 shafts, including 2 cable shafts, a main exhaust air shaft and an access hoisting shaft, which are used for natural ventilation. Hence, there exist mainly two streams of airflow going through this hydro power station as labeled in green and red color respectively, as shown in the Fig.6. The airflow marked as red goes through the transformer hall to cool down the transformer room. The green airflow is directed to the generator room and busbar corridors to dissipate the heat from power generators and high voltage cables. With these airflow characteristics, we build the network model with the schematic shown in Fig.7. In the model, every single space is set as an element and intersections are set as nodes. For the long tunnel, the sub-elements were utilized to capture the temperature changes along the tunnel. The number of sub-elements for

different spaces is indicated in Table 1. The labels of nodes and elements are shown in both Fig.6 and Fig.7. The airflow direction corresponds with the isometric view of power station. The properties of each element of the prototype model are shown in Table 1. It includes the coefficient of flow impedance, the height difference of each element from entrance to exit, the surface area of envelope and volume of each element. The detailed experimental arrangement is illustrated in the Fig.8. Six heat units with 500w normal rated power constituted the local heat sources with a transformer that varied the heat release rate. The Testo 480 climate measurement tool is used to measure the average air velocity over time. A Carbon fiber electric heating cable is used to model the heat released from high voltage cable.

To predict the ventilation status accurately, the established scale model should comply with the similarity theory [49-51]. In this study, the buoyancy-driven natural ventilation that is caused by gravity plays the major role. To achieve the geometric similarity, dynamic similarity and thermal similarity, the Froude and Reynolds numbers should be the same. However, we cannot fulfill these requirements simultaneously. Hence, the Archimedes number is used to achieve the similarity for this experiment [52]. When the geometry scale ratio is 1/20, the airflow rates scale ratio is set to 1/1789 and the scale ratio of heat release rate is 1/1789. Hence, the heat release rate of 635.8 kW per generator is set as 335.4 W in the main powerhouse, while the cables heat release rate of 344.8 kW in the busbar corridor is set as 192.7 W in the scale model. The outdoor temperature is 19.9 °C. In addition, to ensure the performance of the scale model, we have calibrated the heat source control system and thermal anemometer before running the experiments.

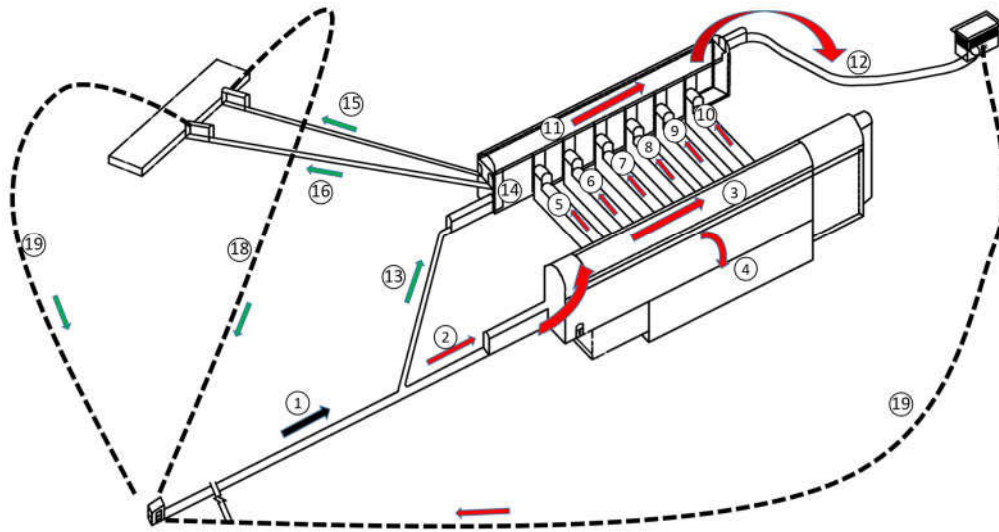


**Fig. 6.** The Isometric view of hydro power station.

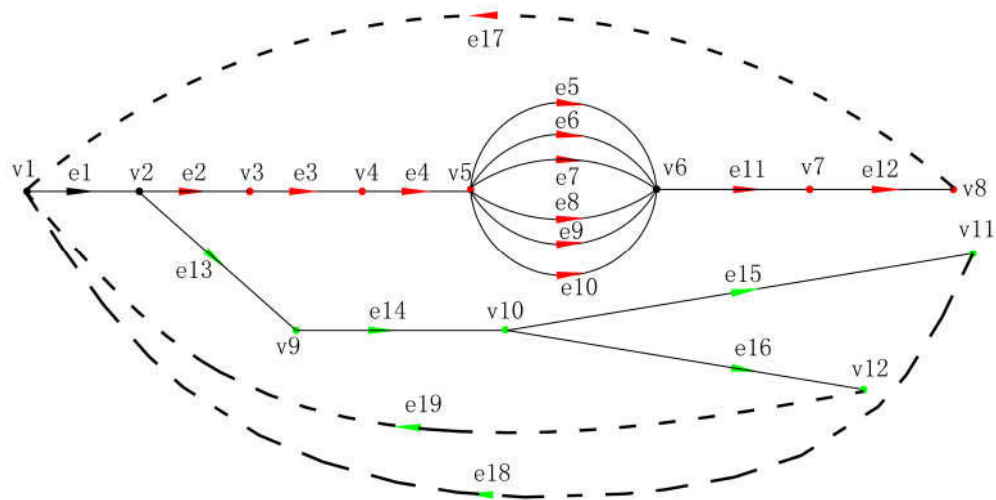


**Fig. 7.** Schematic of the network flow ( e1: Air inlet e2: Access hoist shaft e3:Generator hall e4: Transition floor e5: 1# busbar corridor e6:2# busbar corridor e7: 3# busbar corridor e8:4# busbar corridor e9: 5# busbar corridor e10: 6# busbar corridor e11: Arch roof e12: Main exhaust shaft e13: transportation channel e14: Transformer hall e15: 1#cable outgoing shaft e16: 2#cable outgoing shaft e17-e19: Virtual elements ) .

**Table 1**

Properties of Spaces

No.	U ( $\times 10^{-4} \text{m}^{-4}$ )	Height (m)	Area of envelope ( $\text{m}^2$ )	Air volume ( $\text{m}^3$ )	No. of sub- elements
e1	3.66	-16.37	22942.83	64939.97	5
e2	0.09	-3.38	2977.47	8427.78	1
e3	1.14	-8.25	11406.00	163748.00	1
e4	0	0	6722.69	27284.40	1
e5	235.14	25.25	2166.36	2765.97	1
e6	389.26	25.25	2166.36	2765.97	1
e7	446.83	25.25	2166.36	2765.97	1
e8	899.77	25.25	2166.36	2765.97	1
e9	1120.34	25.25	2166.36	2765.97	1
e10	1114.38	25.25	2166.36	2765.97	1
e11	0	0	5298.21	11493.51	1
e12	13.34	230	11705.01	24709.33	5
e13	5.00	4.030	3047.99	5227.20	2
e14	2.56	11.55	8427.31	29987.09	1
e15	189.20	236.1	9280.20	11949.95	5
e16	186.37	236.1	8672.21	11167.06	5

To investigate the effect of natural ventilation, we have implemented six scenarios of generator operation in the experiment. For each tested scenario, a different number of generators were set as “on” during operation. Since the main purpose of this experiment was to validate the ability of this model to predict the airflow status during natural ventilation, both streams of air flow rates were measured. Because the airflow in long and straight spaces is relatively stable, the natural ventilation rates inside the transformer hall and the generator hall were measured. Fig.9(a) and Fig.9(b) show the comparison of experimental and modeling results for the airflow rates inside element e3(Generator hall) and e14(Transformer hall) under different scenarios. As shown in Fig.9, the relative errors are almost all under 7% while the smallest error is less than 1%. Overall, we can observe that the experimental results are in reasonably good agreement with the network simulation outcomes. However, there are still some limitations to be recognized for this comparison. Firstly, the limitation of similarity, small-scaled models cannot be equivalent to prototypes. Secondly, only the airflow rate is compared, there is no detailed temperature comparison.

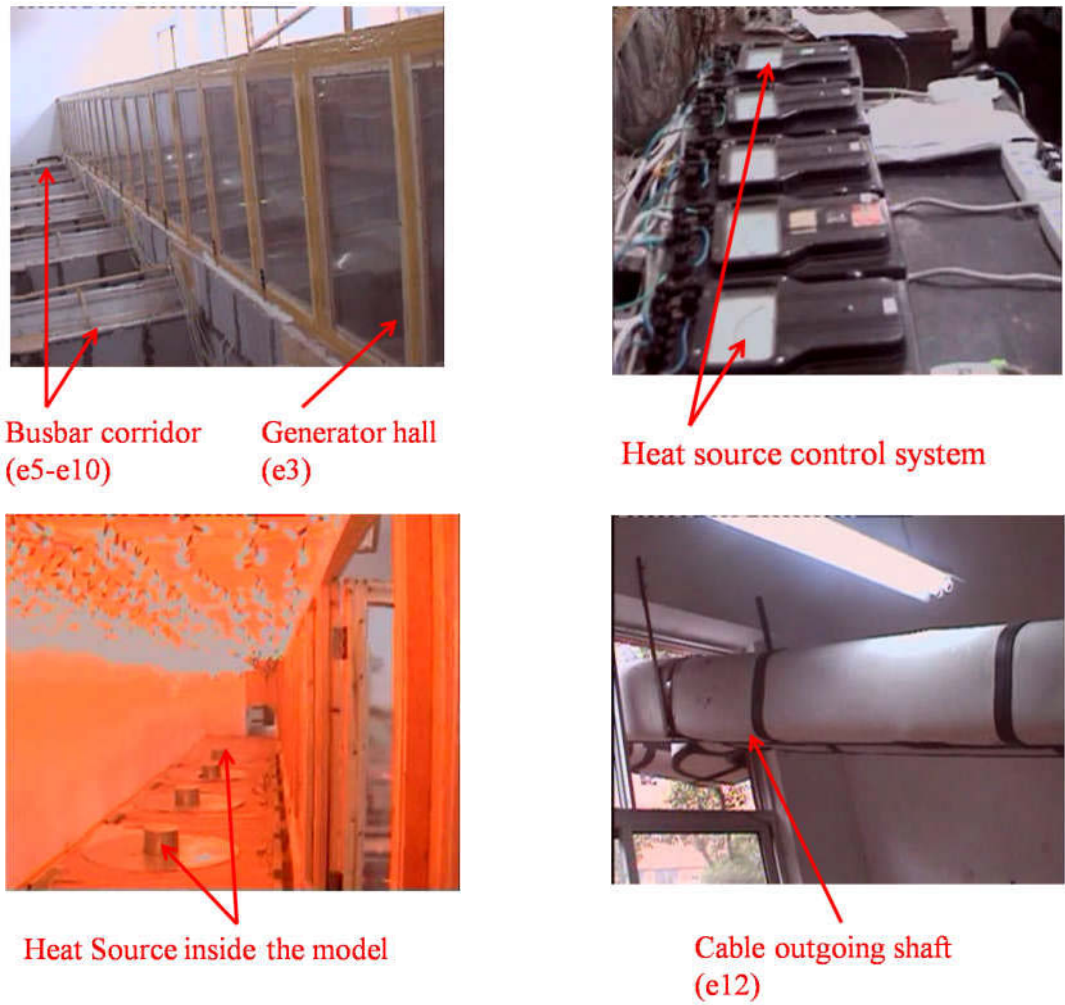


**Fig. 8.** Natural ventilation experiment setup.

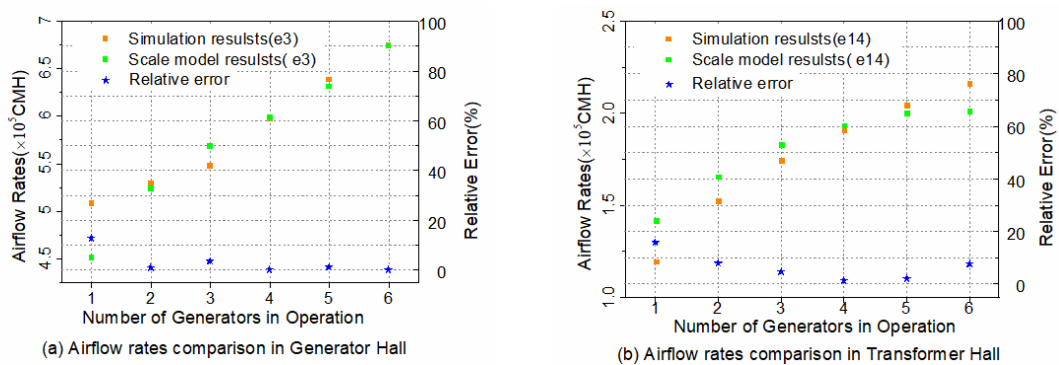


**Fig. 9.** Comparisons of Scale model and simulation results.

### 3.2 Heat transfer model validation (Comparison with field measurements)

As the second phase of validation, the heat transfer model between the airflow and deep rocks was validated using the field measurement in a deep-buried tunnel in Sicuan province, China. The length of tunnel is 305 m with the cross section illustrated in the Fig. 10.

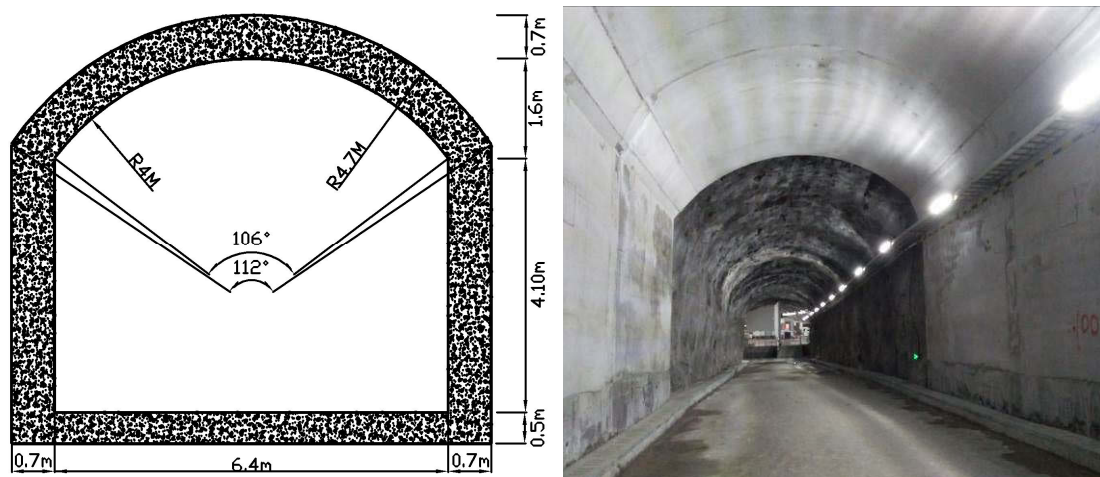


**Fig. 10.** Cross section of the tunnel.

The thermal properties of the tunnel are as follows: The density is  $2800 \text{ kgm}^{-3}$ , the coefficient of conductivity is  $2.80 \text{ Wm}^{-1}\text{K}^{-1}$ , the specific heat is  $900 \text{ Jkg}^{-1}\text{K}^{-1}$ . Outdoor dry-bulb temperature for design condition is  $26.6^\circ\text{C}$ , average yearly temperature is  $11.2^\circ\text{C}$ .

The field measurement period was from July 16<sup>th</sup> to July 21<sup>st</sup>. In the experiment, the Testo 174T mini temperature logger is used to measure the dry-bulb temperature of the inlet and outlet of the tunnel while the Testo 480 climate measurement tool is used to measure the mean air velocity of the tunnel. The measured mean air velocity is about 1.93 m/s. No condensation is observed during the measurement process.

After setting up the measurement environment, we have compared the calculation data

from the established network with the measured data from July 17<sup>th</sup> to July 21<sup>st</sup>. The tunnel is divided into 7 sections with 45 m length for each. Starting from the entrance of air stream, the outlet temperature of the upstream element is taken as the input of the inlet temperature of the downstream element. As observed in the Fig.11, the simulation results are in good agreement with the measurement data both at 180m length and the outlet. In addition, this comparison indicates the accuracy of the dynamic simulation of envelope heat transfer between air and rock. All discrepancies between measured and simulated results are within 1.0°C while the average difference is approximately 0.5°C. The difference between simulated outcomes and measurement on the first day is relatively larger than that on other days. The envelope heat transfer is influenced by the periodical fluctuation of inlet air temperature during previous days. To limit the effect, we start the computation 10 days before, using an identical daily outdoor air temperature profile to limit the influence caused by the period preceding the experiment. In addition, another source of the discrepancy is the assumption of constant air velocity, which is different from the real situation. Finally, the coefficient of thermal conductivity of the rock is not uniform along the tunnel due to small variations in materials used during construction, while the area of the actual internal cross section may differ along the tunnel as well. All these differences could result in (small) deviations.

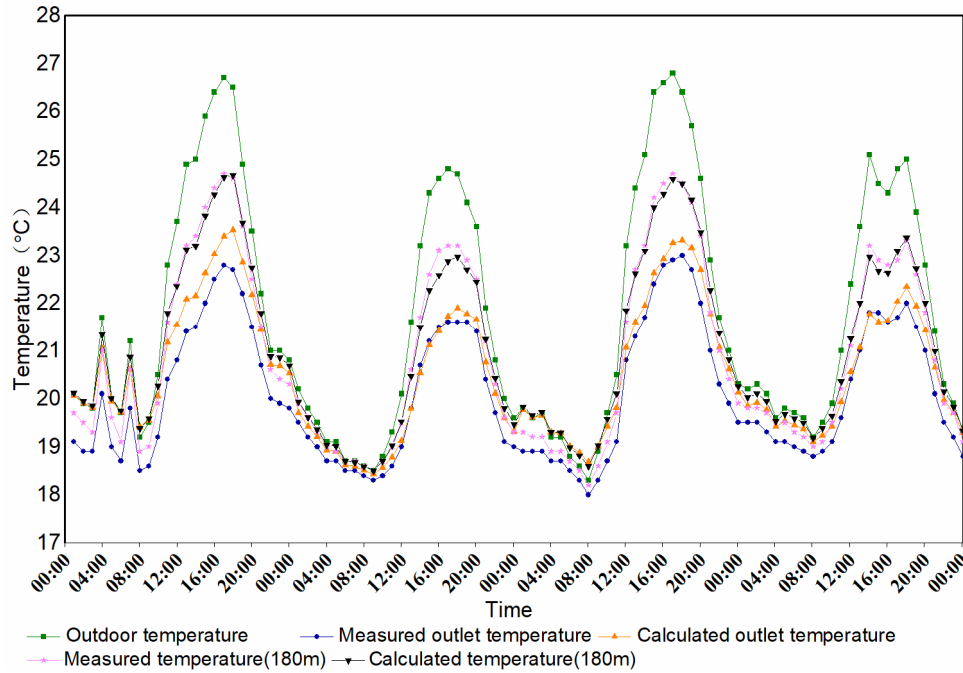


**Fig. 11.** Comparison between simulations and field measurements.

#### 4. Discussion of elements division

For the sizing of elements, it is obvious that the smaller the element, the more accurate it is, but this will increase the computational burden. The rate of air temperature change along the length should be considered. The more gradual the temperature change, the larger the unit length should be. We reproduce the air temperature distribution along the tunnel length for [43] as shown in Fig.12. Alternatively, we divide the tunnel into 20m length per segment. In the reference case, the temperature change in the first 20m is  $0.2^{\circ}\text{C}$ , while at the end of the tunnel the temperature change is  $0.02^{\circ}\text{C}$ . Comparing the results of thermal pressure along the tunnel length, in the first 20m, the relative error is 0.4%; in the last 20m, the relative error is 0.0005%; in the whole tunnel, the relative error is 0.003%. When we increase the length to 100m, the temperature change in the first 100m is  $0.9^{\circ}\text{C}$ , while at the end of the tunnel the temperature change is  $0.1^{\circ}\text{C}$ . Comparing the results of thermal pressure, in the first 100m, the relative error is 2.16%; in the last 100m, the relative error is 0.014%; in the whole tunnel, the relative error is

0.08%.

Based on the sensitivity analysis, the temperature variation of the airflow is significant within the first 100m. But the relative error of thermal pressure calculation is within acceptable accuracy (2.16 %) even with an element size of 100m. Hence, in the buoyancy ventilation of underground buildings, the size of an element should be smaller at the inlet of the tunnel. After the first 100m, the element length could be increased to reduce the computational burden.

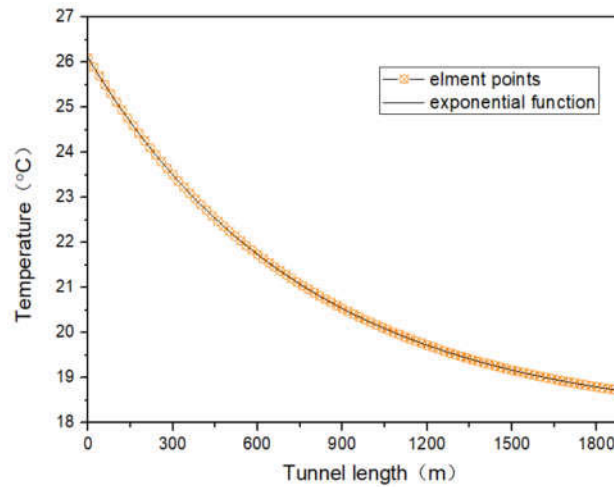


**Fig. 12.** Temperatures distributing model.

The airflow in the large underground spaces are much more complicated than in long tunnels. If the assumptions of the element division do not match the actual situation, it will lead to errors. The same problem also exists in other multizone network models; some assumptions for the models, such as one-dimensional airflow, well-mixed temperature, will cause errors [53]. The temperature distribution in the element of underground space is influenced by the internal heat sources, the position of inlet and outlet and the airflow. On the other hand, the temperature distribution in the element will affect the airflow through the buoyancy effect. Once the way of element division is provided, the corresponding relationship between heat source and element, the path of airflow and the temperature distribution inside the element is confirmed, which may be different from the actual situation. Therefore, the different division of elements may affect the ventilation calculation results. As shown in the Fig.13 (a), two ways of

elements division for a large space will produce two different network structures, and may lead to different calculation results. Therefore, further research should be carried out regarding the method of element division of large underground spaces.

In a real project, when the height difference between the entrance and exit of the large underground space is smaller than that of the long tunnel leading to the outdoor, it can be considered as one element. The calculation of airflow rates in the main path of the whole network is acceptable, although the description of temperature and airflow distribution in a large space may be quite different from the actual situation. For example, the height difference between the inlet and outlet of the generator hall (e3) is 8.25 m, which only accounts for 3.6% of the height difference of the main exhaust shaft (e12) and 3.5% of the height difference of the cable-outgoing shaft (e15). Therefore, the thermal effect caused by the spatial temperature distribution has minor influence on the overall ventilation flow. Therefore, for similar practical engineering problems, the one-dimensional model can calculate the overall ventilation status, followed by the field model to analyze detailed airflow and temperature distributions in the large spaces.

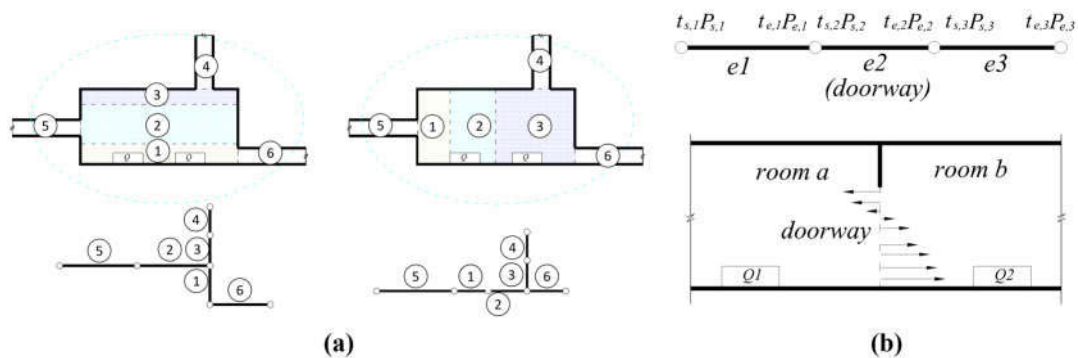


**Fig. 13.** Element division: (a) Different way of element division for large space ;( b) Element division for large opening.

Airflows through large openings (e.g. doorways) are complex with the possibility of flows in opposite directions in different parts of the opening. The temperature and resulting density difference between two rooms may mean that the buoyancy effect causes a positive pressure difference at the top of the doorway and a negative pressure

difference at the bottom(or vice versa) thus leading to a two-way flow in the opening [54-57]. In our proposed model, to solve the two-way airflow through the doorway, individual element is employed for the doorway itself as illustrated in Fig.13 (b). This element: (1) Has no volume; (2) Has flow resistance (comply with Eq.2-3). The temperature, flow rate and flow resistance of each element is obtained by solving the network model. Then, the pressure at the end of each element could be obtained. Combining with the geometrical and topological information of the doorway and adjacent space, the airflow through the doorway is calculated by employing the Single Opening Model of CONTAM [57]. If the net airflow rates are consistent with the results in the network model, we proceed to the next time step. If the results of the Single Opening Model do not agree with those of the network model, then the flow impedance coefficient of the doorway should be modified. And the network model is calculated again. The process is repeated until the results are within acceptable accuracy. Then, the next time step is carried out.

## **5. Conclusions**

For underground structures that are buried deep and only connected by channels to the surface, it has been argued that conventional multizone airflow modeling methods are not suitable for natural ventilation analysis in complex configuration containing tunnels in which the airflow is predominantly one-dimensional. To respond to this challenge, this paper describes a new type of one-dimensional network model that integrates a flow network and a thermal network model to simulate natural ventilation of underground buildings. The pressure balance of the loops and mass flow balance of the nodes are considered to form the network flow model equations. Heat balance of elements, heat balance equations for airflows mixing process at the node, isothermal equations and heat transfer equations of envelope are incorporated to build the full thermal network model, which is computationally solved to predict the dynamic response of natural ventilation. This model is designed to be widely applicable in the investigation of natural ventilation, mechanical ventilation, hybrid ventilation and fire

smoke ventilation.

A validation was performed to verify the model simulation accuracy and demonstrate its application. In the validation, natural ventilation of an underground hydro power station under different operation conditions was simulated to generate different ventilation rates. The comparison of laboratory and simulated results indicates that the steady-state airflows are in good agreements. In addition, the integrated model for simulating the heat transfer between rocks and airflow in caverns is validated through comparison between simulations and field measurements.

The proposed approach has some limitations that call for future work. First, the flow impedance coefficients that are required as basic input parameters are generally unknown. Tests with scale models could be used to estimate them but that would be impractical to do for every case, which may involve many proposed alternative designs. However, due to the complexities of geometry, currently, the only established way to obtain the flow impedance coefficients is through a scale model test. A better way would be to generate empirical relationships based on configuration and other parameters. However, large amounts of tests and theoretical studies are necessary to derive an empirical formula that estimates the impedance coefficient accurately. Second, the network model is not capable of delivering the detailed temperature and airflow distribution inside the caverns. A full-scaled CFD simulation could deliver those, but this would result in significant amounts of computational burden. Hence, we propose to conduct future work to combine CFD with the proposed network model in order to consider the complexities of heat sources and airflow patterns inside (large) spaces with limited amount of mixing. As a final limitation, we should mention that we have not studied the effect of humidity. It should be realized that the humidity could be a vital aspect in controlling the environment in underground structures.

## Acknowledgement

The authors acknowledge the support from National Natural Science Foundation of China (NSFC) (51678088, 51178482, 51578087). Yanan Liu also especially thanks for the scholarship provided by China Scholarship Council (CSC student ID:201706050003).

## Appendix A Derivation of coefficient matrix for the heat balance equations for airflows mixing process at the node

When we generate the ventilation network, we can assume the direction of an element first. The value of airflow rate is positive when the direction of the airflow is the same as that of the element, and vice versa. The incidence matrix of actual flow direction is established according to the actual flow direction in the element. Based on the incident matrix  $A$ , the actual incidence matrix  $A_m$  can be formed according to the real flow direction. Its calculation could be expressed as below:

$$A_m = A \times \text{diag} \left( \frac{M_j}{|M_j|} \right) \quad (\text{A1})$$

Where  $M_j$  is Mass flow rate of the  $j$ th element,  $\text{diag} \left( \frac{M_j}{|M_j|} \right)$  is  $n \times n$  diagonal matrix with diagonal entries as  $\frac{M_j}{|M_j|}$ .

$A_m$  has  $m$  rows and  $n$  columns. In the matrix, each column corresponds to one element. Hence, there are at least two non-zero entries 1 and -1, which indicate the start and end of that element. Meanwhile, each row corresponds to one node. Similarly, there are at least two non-zero entries 1 and -1 that stand for the inflow and outflow as well.

$$\text{diag} \left( \frac{M_j}{|M_j|} \right) = \begin{bmatrix} \frac{M_1}{|M_1|} & 0 & 0 & \cdots & 0 \\ 0 & \frac{M_2}{|M_2|} & 0 & \cdots & 0 \\ 0 & 0 & \ddots & 0 & \vdots \\ \vdots & \vdots & 0 & \ddots & 0 \\ 0 & 0 & \cdots & 0 & \frac{M_n}{|M_n|} \end{bmatrix} \quad (\text{A2})$$

Two new matrices,  $A_1$  and  $A_2$ , are introduced, and their elements  $x_{ij}$  and  $z_{ij}$  are defined as:

$$\begin{cases} x_{ij} = 1 \text{ when } i_j = 1; \\ x_{ij} = 0 \text{ when } i_j \neq 1; \end{cases} \quad (\text{A3})$$

$$\begin{cases} z_{ij} = -1, \text{ when } i_j = -1; \\ z_{ij} = 0, \text{ when } i_j \neq -1; \end{cases} \quad (\text{A4})$$

The rows of  $A_{x1}$  correspond to the node label and the columns of  $A_{x1}$  corresponds to the element label of the network. Both  $A_1$  and  $A_{x2}$  reflect the flow direction between the node and the element connected to it. For example,  $x_{ij} = 1$  means the flow exists from the  $i^{\text{th}}$  node to the  $j^{\text{th}}$  element; while  $z_{ij} = -1$  means the flow enters the  $i^{\text{th}}$  node from the  $j^{\text{th}}$  element.

$A_{je}$  and  $A_{ji}$  are correlated with  $A_1$  and  $A_2$ , respectively, given by:

$$\begin{cases} A_{je} = A_1 \cdot \text{diag}(|M_j|); \\ A_{ji} = A_{x2} \cdot \text{diag}(|M_j|); \end{cases} \quad (\text{A5})$$

The coefficient matrix of heat balance equations is expressed as:

$$A_{jr} = [A_{je}; A_{ji}] \quad (\text{A6})$$

## Appendix B Derivation of coefficient matrix for the isothermal equations

As described in Appendix A, if  $x_{ij} = 1$ , it represents that the outflow of the  $j^{\text{th}}$  element exists the  $i^{\text{th}}$  node. For the  $i^{\text{th}}$  row of  $A_1$ , if  $g_i = \sum_{j=1}^n x_{ij} \geq 2$ , it represents that the quantity of the outflow element of the  $i^{\text{th}}$  node is no less than 2, and thus  $g_i - 1$  isothermal equations of node outflow can be established.

For the row of  $A_{x1}$  which meets  $g_i \geq 2$ , a diagonal matrix,  $\text{diag}[a_{ij}]$ , can be

established, which is composed of the elements of  $a_{ij}$  corresponding to the  $i^{th}$  node. In each  $\text{diag}[a_{x1ij}]$ ,  $g_i - 1$  row vector can be obtained by subtracting the rows that contains the element of 1 from the row where the element 1 first occurs. Then,  $\sum_{i=1}^m (g_i - 1) = n - m$  row vectors can be obtained from operations above, and they constitute a new matrix with the order of  $(n - m) \times n$ ,  $A_{jc1}$ . Then, the isothermal equations can be expressed in a simplified matrix form, given by:

$$A_{jc} \cdot T = 0 \quad (\text{A7})$$

Where

$$A_{jc} = [A_{jc1}; \text{zeros}(n - mn)] \quad (\text{A8})$$

## Figure captions

Fig.1. Schematical comparison between underground building and aboveground building

Fig.2. Schematic of an element

Fig.3. A typical natural ventilation network of deep-buried underground building

Fig. 4. Coupling between unknown parameters

Fig. 5. Diagram of the solution process

Fig.6. The Isometric view of hydro power station

Fig.7. Schematic of the network flow ( e1: Air inlet e2: Access hoist shaft e3:Generator hall e4: Transition floor e5: 1# busbar corridor e6:2# busbar corridor e7: 3# busbar corridor e8:4# busbar corridor e9: 5# busbar corridor e10: 6# busbar corridor e11: Arch roof e12: Main exhaust shaft e13: transportation channel e14: Transformer hall e15: 1#cable outgoing shaft e16: 2#cable outgoing shaft e17-e19: Virtual elements )

Fig.8. Natural ventilation experiment setup

Fig. 9. Comparisons of Scale model and simulation results

Fig. 10. Cross section of the tunnel

Fig. 11. Comparison between simulations and field measurements

Fig. 12. Temperatures distributing model

Fig. 13. Element division: (a) Different way of element division for large space; (b)

Element division for large opening.

## Table captions

Table 1. Properties of Spaces

## References

[1] Zhao, Y., Yoshino, H., & Okuyama, H. (1998). Evaluation of the COMIS model by comparing simulation and measurement of airflow and pollutant concentration. *Indoor Air*, 8(2), 123-130.

DOI: <https://doi.org/10.1111/j.1600-0668.1998.t01-2-00007.x>

[2] Mora-Pérez, M., Guillén-Guillamón, I., & López-Jiménez, P. A. (2015). Computational analysis of wind interactions for comparing different buildings sites in terms of natural ventilation. *Advances in Engineering Software*, 88, 73-82.

DOI: <https://doi.org/10.1016/j.advensoft.2015.06.003>

[3] Tong, Z., Chen, Y., & Malkawi, A. (2017). Estimating natural ventilation potential for high-rise buildings considering boundary layer meteorology. *Applied energy*, 193, 276-286.

DOI: <https://doi.org/10.1016/j.apenergy.2017.02.041>

[4] Tong, Z., Chen, Y., & Malkawi, A. (2016). Defining the Influence Region in neighborhood-scale CFD simulations for natural ventilation design. *Applied Energy*, 182, 625-633.

DOI: <https://doi.org/10.1016/j.apenergy.2016.08.098>

[5] Ding, C., He, X., & Nie, B. (2017). Numerical simulation of airflow distribution in mine tunnels. *International Journal of Mining Science and Technology*, 27(4), 663-667.

DOI: <https://doi.org/10.1016/j.ijmst.2017.05.017>

[6] Stephan, L., Bastide, A., & Wurtz, E. (2011). Optimizing opening dimensions for naturally ventilated buildings. *Applied Energy*, 88(8), 2791-2801.

DOI: <https://doi.org/10.1016/j.apenergy.2010.12.039>

[7] Wang, H., & Zhai, Z. J. (2016). Advances in building simulation and computational techniques: A review between 1987 and 2014. *Energy and Buildings*, 128, 319-335.

DOI: <https://doi.org/10.1016/j.enbuild.2016.06.080>

[8] Chen, Q. (2009). Ventilation performance prediction for buildings: A method overview and recent applications. *Building and environment*, 44(4), 848-858.

DOI: <https://doi.org/10.1016/j.buildenv.2008.05.025>

[9] Li, Y., & Delsante, A. (2001). Natural ventilation induced by combined wind and thermal forces. *Building and Environment*, 36(1), 59-71. DOI: [https://doi.org/10.1016/S0360-1323\(99\)00070-0](https://doi.org/10.1016/S0360-1323(99)00070-0)

- [10] Hayden, C. S., Earnest, G. S., & Jensen, P. A. (2007). Development of an empirical model to aid in designing airborne infection isolation rooms. *Journal of occupational and environmental hygiene*, 4(3), 198-207. DOI: <https://doi.org/10.1080/15459620601177370>
- [11] Feustel, H. E., & Dieris, J. (1992). A survey of airflow models for multizone structures. *Energy and buildings*, 18(2), 79-100. DOI: [https://doi.org/10.1016/0378-7788\(92\)90040-N](https://doi.org/10.1016/0378-7788(92)90040-N)
- [12] Feustal, H. E., Allard, F., Dorer, V., Garcia, E. R., Herrlin, M., Grosso, M., ... & Yoshino, H. (1990). COMIS fundamentals.
- [13] Feustel, H. E. (1999). COMIS—an international multizone air-flow and contaminant transport model. *Energy and Buildings*, 30(1), 3-18. DOI: [https://doi.org/10.1016/S0378-7788\(98\)00043-7](https://doi.org/10.1016/S0378-7788(98)00043-7)
- [14] Grosso, M. (1992). Wind pressure distribution around buildings: a parametrical model. *Energy and Buildings*, 18(2), 101-131. DOI: [https://doi.org/10.1016/0378-7788\(92\)90041-E](https://doi.org/10.1016/0378-7788(92)90041-E)
- [15] Haghghat, F., & Megri, A. C. (1996). A comprehensive validation of two airflow models—COMIS and CONTAM. *Indoor air*, 6(4), 278-288. DOI: <https://doi.org/10.1111/j.1600-0668.1996.00007.x>
- [16] Sohn, M. D., Apte, M. G., Sextro, R. G., & Lai, A. C. (2007). Predicting size-resolved particle behavior in multizone buildings. *Atmospheric Environment*, 41(7), 1473-1482. DOI: <https://doi.org/10.1016/j.atmosenv.2006.10.010>
- [17] Wang, L., & Chen, Q. (2008). Applications of a coupled multizone-cfd model to calculate airflow and contaminant dispersion in built environments for emergency management. *HVAC&R Research*, 14(6), 925-939. DOI: <https://doi.org/10.1080/10789669.2008.10391047>
- [18] Wang, L., & Chen, Q. (2007). Theoretical and numerical studies of coupling multizone and CFD models for building air distribution simulations. *Indoor Air*, 17(5), 348-361. DOI: <https://doi.org/10.1111/j.1600-0668.2007.00481.x>
- [19] Wang, L. L., Dols, W. S., & Chen, Q. (2010). Using CFD capabilities of CONTAM 3.0 for simulating airflow and contaminant transport in and around buildings. *Hvac&R Research*, 16(6), 749-763. DOI: <http://dx.doi.org/10.1080/10789669.2010.10390932>
- [20] Tan, G., & Glicksman, L. R. (2005). Application of integrating multi-zone model with CFD simulation to natural ventilation prediction. *Energy and Buildings*, 37(10), 1049-1057. DOI: <http://dx.doi.org/10.1016/j.enbuild.2004.12.009>
- [21] Wang, L., & Chen, Q. (2007). Validation of a coupled multizone-CFD program for building airflow and contaminant transport simulations. *HVAC&R Research*, 13(2), 267-281. DOI: <http://dx.doi.org/10.1080/10789669.2007.10390954>
- [22] Wang, L., & Chen, Q. (2005, August). On solution characteristics of coupling of multizone and CFD programs in building air distribution simulation. In *Proceedings of Building Simulation (Vol. 5, pp. 1315-1322)*.
- [23] Tan, G. (2005). Study of natural ventilation design by integrating the multi-zone model with CFD simulation (Doctoral dissertation, Massachusetts Institute of Technology).
- [24] Parker, S. T., & Bowman, V. (2011). State-space methods for calculating concentration dynamics in multizone buildings. *Building and Environment*, 46(8), 1567-1577. DOI: <https://doi.org/10.1016/j.buildenv.2011.01.016>

- [25] Axley, J. (2007). Multizone airflow modeling in buildings: History and theory. *HVAC&R Research*, 13(6), 907-928. DOI: <https://doi.org/10.1080/10789669.2007.10391462>
- [26] Savić, D. A., & Walters, G. A. (1996). Integration of a model for hydraulic analysis of water distribution networks with an evolution program for pressure regulation. *Computer - Aided Civil and Infrastructure Engineering*, 11(2), 87-97.  
DOI:<https://doi.org/10.1111/j.1467-8667.1996.tb00313.x>
- [27] Fytas, K., & Perreault, S. (2002, February). EOLAVAL- a mine ventilation planning software. In *APCOM 2002: 30 th International Symposium on the Application of Computers and Operations Research in the Mineral Industry* (pp. 413-421).
- [28] Fytas, K., Perreault, S., & Daigle, B. (2018). EOLAVAL, a mine ventilation planning tool. In *Mine Planning and Equipment Selection 2000* (pp. 51-56). Routledge.
- [29] Jensen, R. L., Grau, K., & Heiselberg, P. K. (2007). Integration of a multizone airflow model into a thermal simulation program. *Building Simulation*.
- [30] Li, A., Gao, X., & Ren, T. (2017). Study on thermal pressure in a sloping underground tunnel under natural ventilation. *Energy and Buildings*, 147, 200-209.  
DOI:<https://doi.org/10.1016/j.enbuild.2017.04.060>
- [31] Li, A., Qin, E., Xin, B., Wang, G., & Wang, J. (2010). Experimental analysis on the air distribution of powerhouse of Hohhot hydropower station with 2D-PIV. *Energy Conversion and Management*, 51(1), 33-41.  
DOI:<https://doi.org/10.1016/j.enconman.2009.08.022>
- [32] Yu, Y., Cao, L., Li, X., Shi, W., & Wu, J. (2015). Modeling of heat and mass transfer of tunnel ventilation in hydropower station. *Applied Thermal Engineering*, 90, 45-53.  
DOI:<https://doi.org/10.1016/j.applthermaleng.2015.06.097>
- [33] Liu, Y., Wang, S., Deng, Y., Ma, W., & Ma, Y. (2016). Numerical simulation and experimental study on ventilation system for powerhouses of deep underground hydropower stations. *Applied Thermal Engineering*, 105, 151-158.  
DOI:<https://doi.org/10.1016/j.applthermaleng.2016.05.101>
- [34] Cheng, J., Wu, Y., Xu, H., Liu, J., Yang, Y., Deng, H., & Wang, Y. (2015). Comprehensive and integrated mine ventilation consultation model—CIMVCM. *Tunnelling and Underground Space Technology*, 45, 166-180.  
DOI:<https://doi.org/10.1016/j.tust.2014.09.004>
- [35] Szlązak, N., Obracaj, D., & Korzec, M. (2017). Analysis of connecting a forcing fan to a multiple fan ventilation network of a real-life mine. *Process Safety and Environmental Protection*, 107, 468-479.  
DOI:<https://doi.org/10.1016/j.psep.2017.03.001>
- [36] Lin, C. J., Chuah, Y. K., & Liu, C. W. (2008). A study on underground tunnel ventilation for piston effects influenced by draught relief shaft in subway system. *Applied Thermal Engineering*, 28(5-6), 372-379.  
DOI:<https://doi.org/10.1016/j.applthermaleng.2007.10.003>
- [37] Pan, S., Fan, L., Liu, J., Xie, J., Sun, Y., Cui, N., ... & Zheng, B. (2013). A review of the piston effect in subway stations. *Advances in Mechanical Engineering*, 5, 950205.  
DOI:<https://doi.org/10.1155/2013/950205>

- [38] Krasnyuk, A. M. (2005). Calculation of tunnel ventilation in shallow subways. *Journal of Mining Science*, 41(3), 261-267.  
DOI:<https://doi.org/10.1007/s10913-005-0090-4>
- [39] Huang Fuqi, Zhang Jiayou, Xie Shoumu, et al. (1983). *The Thermal Calculation Method of Underground Engineering*, China Architecture and Building Press, Beijing.(In Chinese)
- [40] Xiao, Y., Liu, X., & Zhang, R. (2012). Calculation of transient heat transfer through the envelope of an underground cavern using Z-transfer coefficient method. *Energy and Buildings*, 48, 190-198.  
DOI:<https://doi.org/10.1016/j.enbuild.2012.01.040>
- [41]. Qi, D., Wang, L., & Zmeureanu, R. (2014). An analytical model of heat and mass transfer through non-adiabatic high-rise shafts during fires. *International Journal of Heat and Mass Transfer*, 72, 585-594.  
DOI: <http://dx.doi.org/10.1016/j.ijheatmasstransfer.2014.01.042>
- [42]. Qi, D., Wang, L., & Zmeureanu, R. (2015). Modeling smoke movement in shafts during high-rise fires by a multizone airflow and energy network program. *ASHRAE Transactions*, 121(2).
- [43].Li, A., Gao, X., & Ren, T. (2017). Study on thermal pressure in a sloping underground tunnel under natural ventilation. *Energy and Buildings*, 147, 200-209.  
DOI: <https://doi.org/10.1016/j.enbuild.2017.04.060>
- [44] Blandford, T. R., Humes, K. S., Harshburger, B. J., Moore, B. C., Walden, V. P., & Ye, H. (2008). Seasonal and synoptic variations in near-surface air temperature lapse rates in a mountainous basin. *Journal of Applied Meteorology and Climatology*, 47(1), 249-261.  
DOI: <https://doi.org/10.1175/2007JAMC1565.1>
- [45] Y.M. Xiao(2005).Network simulation and application of natural ventilation in underground spaces of hydropower stations.( PhD Thesis, Chongqing University, In Chinese)
- [46] Awbi, H. B. (2002). *Ventilation of buildings*. Routledge.
- [47]Yang, H., Wen, F., Wang, L., & Singh, S. N. (2008, December). Newton-downhill algorithm for distribution power flow analysis. In *Power and Energy Conference, 2008. PECon 2008. IEEE 2nd International* (pp. 1628-1632). IEEE.  
DOI: <https://doi.org/10.1109/PECON.2008.4762740>
- [48] Li, Q., Guan, Z., & Bai, F. (2000). *The principle of numerical methods*. Beijing: Tsinghua University Press. In Chinese.
- [49] Le Roux, N., Faure, X., Inard, C., Soares, S., & Ricciardi, L. (2012). Reduced-scale study of wind influence on mean airflows inside buildings equipped with ventilation systems. *Building and Environment*, 58, 231-244  
DOI:<https://doi.org/10.1016/j.buildenv.2012.07.007>
- [50] Le Roux, N., Faure, X., Inard, C., Soares, S., & Ricciardi, L. (2013). Reduced-scale study of transient flows inside mechanically ventilated buildings subjected to wind and internal overpressure effects. *Building and Environment*, 62, 18-32.  
DOI:<https://doi.org/10.1016/j.buildenv.2013.01.011>
- [51] Huang, H., & Yan, Z. (2009). Present situation and future prospect of hydropower in China. *Renewable and Sustainable Energy Reviews*, 13(6-7), 1652-1656.

DOI:<https://doi.org/10.1016/j.rser.2008.08.013>

[52] Ren, T., Li, A., Luo, N., & Zhang, Y. (2016). 1: 50 scale modeling study on airflow effectiveness of large spaces mutually connected for underground workshops. *Building Simulation* 9(2), 201-212.

DOI:<https://doi.org/10.1007/s12273-015-0258-z>

[53]. Wang, L. L., & Chen, Q. (2008). Evaluation of some assumptions used in multizone airflow network models. *Building and Environment*, 43(10), 1671-1677.

DOI: <https://doi.org/10.1016/j.buildenv.2007.10.010>

[54]. Allard, F., & Utsumi, Y. (1992). Airflow through large openings. *Energy and Buildings*, 18(2), 133-145.

DOI: [https://doi.org/10.1016/0378-7788\(92\)90042-F](https://doi.org/10.1016/0378-7788(92)90042-F)

[55]. Barakat, S. A. (1987). Inter-zone convective heat transfer in buildings: a review. *Journal of solar energy engineering*, 109(2), 71-78.

DOI:<https://doi.org/10.1115/1.3268195>

[56]. Brown, W. G., & Solvason, K. R. (1962). Natural convection through rectangular openings in partitions—1: Vertical partitions. *International Journal of Heat and Mass Transfer*, 5(9), 859-868.

DOI: [https://doi.org/10.1016/0017-9310\(62\)90184-9](https://doi.org/10.1016/0017-9310(62)90184-9)

[57]. Dols, W. S., & Polidoro, B. J. (2015). CONTAM User Guide and Program Documentation Version 3.2 (No. Technical Note (NIST TN)-1887).